International Journal of Microwave and Wireless Technologies

cambridge.org/mrf

A flat-gain MIMO antenna design utilizing joint excitation of patch antenna and metasurface for TM_{10} mode

Jinrong Su[1,2], Shiqi Di[1], Xinwei Chen[1,2], Runbo Ma[1,2] and Wenmei Zhang[1,2]

[1]School of Physics and Electronic Engineering, Shanxi University, Taiyuan, China and [2]Shanxi Key Laboratory of Wireless Communication and Detection, Shanxi University, Taiyuan, China

Research Paper

Cite this article: Su J, Di S, Chen X, Ma R, Zhang W (2026) A flat-gain MIMO antenna design utilizing joint excitation of patch antenna and metasurface for TM_{10} mode. *International Journal of Microwave and Wireless Technologies* **18**(2), 250–261. https://doi.org/10.1017/S1759078726102943

Received: 9 September 2025
Revised: 26 January 2026
Accepted: 26 January 2026

Keywords
characteristic modes analysis; flat-gain; metasurface; multiple-input multiple-output

Corresponding author: Jinrong Su; Email: sujinrong@sxu.edu.cn

Abstract

This paper presents a broadband metasurface (MS) antenna designed through characteristic modes analysis. By introducing horizontal slots into a 3 × 3 MS array, a pair of degenerate modes is successfully separated and the dominant mode is reconfigured as TM_{10} mode. Optimizing feed position simultaneously excites the TM_{10} modes of both the patch antenna and the MS, expanding the −10 dB impedance bandwidth from 4.09–4.22 GHz to 3.45–4.5 GHz with a gain variation of less than 1.9 dB. Furthermore, a dual-port multiple-input multiple-output (MIMO) antenna is constructed by orthogonally arranging two elements. The exclusive TM_{10} mode enables inherent decoupling, achieving over 23.6 dB isolation. Measured results exhibit good agreement with simulations, demonstrating an operational band of 3.44–4.39 GHz, effectively covering the 5G NR (New Radio) n48 band.

Introduction

The evolution of the fifth generation (5G) mobile communication technology escalates the demands for spectrum resources and data transmission rates. Multiple-input multiple-output (MIMO) technology is central to meeting this demand by increasing channel capacity, which is typically achieved by deploying more antenna elements within a limited space. However, this dense integration inevitably intensifies mutual coupling between elements, degrading system performance. Consequently, achieving effective decoupling without sacrificing compactness constitutes a fundamental challenge in MIMO antenna design [1, 2, 27].

In recent years, various methods have been proposed to mitigate the mutual coupling between MIMO antenna elements. Representative approaches include coupling suppression through structural modifications such as defected ground structures (DGSs) [3], metamaterial configurations [4], and coupling cancellation utilizing neutralization lines [5], or parasitic decoupling structures between radiating elements [6, 7]. While effective, these approaches often increase design complexity and footprint. To address spatial constraints, self-decoupling techniques have emerged as a promising alternative [8–12]. For example, a differential feeding technique enables over 40 dB self-decoupling [8]. Hussain et al. achieve over 30 dB isolation through polarization diversity [9]. A key self-decoupling strategy exploits inherent modal properties. For example, characteristic mode analysis has been applied to guide structural evolution, achieving isolation greater than 24 dB [10]. Alternatively, exciting specific orthogonal modes (TM_{10} and TM_{02}) in excited and non-excited elements has also proven effective [11, 12]. Despite these significant advancements in isolation, persistent challenges such as narrow bandwidth and insufficient compactness remain critical limitations for further investigation.

To overcome the narrowband limitations of patch antennas, researchers have proposed metasurface (MS)-integrated MIMO configurations. These designs utilize the unique electromagnetic properties of MSs to broaden bandwidth and enhance isolation. A common approach is to place an MS decoupling array above the radiating patches, which improves isolation but often requires an air gap that increases the profile [13–16, 25, 26]. To achieve a lower profile, MSs composed of periodic split-ring resonators [14] or square cells [17] have been integrated around patch antennas, achieving isolations greater than 25 and 30 dB respectively. Beyond the traditional periodic analysis method MS design, research on self-decoupling MS antennas based on characteristic modes analysis (CMA) has also emerged. For example, CMA has been used to achieve self-decoupling via mode separation and higher-order mode suppression [18]. Ding et al. excited four orthogonal radiation modes through CMA, realizing over 20 dB isolation [19]. Zeng et al. introduced a set of metal vias into a densely arranged MS MIMO structure to control the mode electric fields of non-excited elements, thereby achieving self-decoupling through electric field cancellation [20]. Li et al. applied CMA and shaping techniques to suppress coupling modes for self-decoupling, achieving an isolation of up to 45 dB [23].

© The Author(s), 2026. Published by Cambridge University Press in association with The European Microwave Association.

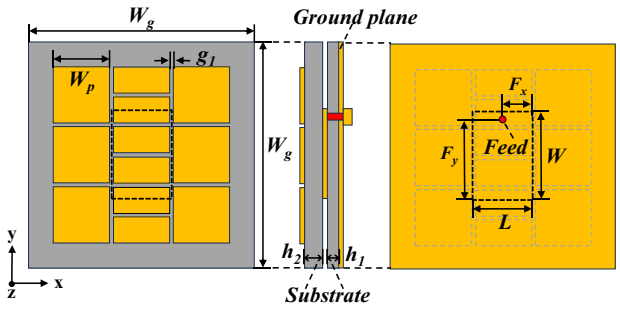


Figure 1. Geometry of the single-port MS MIMO antenna.

Table 1. The dimension parameters of antenna

Parameters	Value/mm	Parameters	Value/mm	Parameters	Value/mm
L_g	75	W_g	40	W_p	10
g_1	0.7	L	11	W	16
g_2	4.3	F_x	5.5	F_y	14.8
h_1	1.8	h_2	3	L_p	11.65
W_d	14.5				

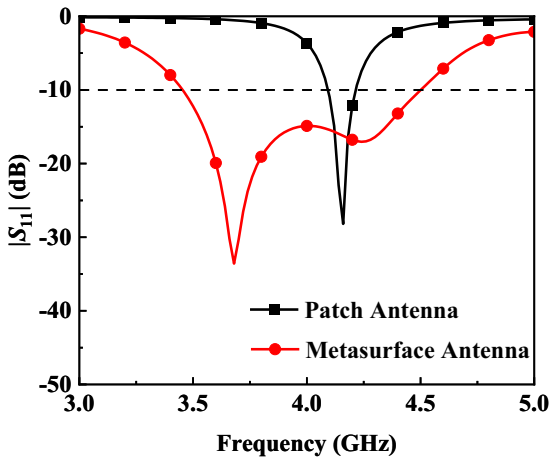


Figure 2. The simulated *S*-parameters of the patch antenna with and without MS.

While these MS-based methods have yielded significant decoupling effects, their overall footprints and profiles still require further optimization.

In this paper, a compact MS antenna with flat gain is proposed based on CMA. The antenna comprises an intimately integrated MS layer and a rectangular patch antenna, forming a low-profile structure with optimized compactness. Horizontal slots in the central MS units separate and reconfigure the dominant mode. A coaxial feed then simultaneously excites the TM_{10} modes of both the patch and the MS, yielding a −10 dB impedance bandwidth from 3.45 to 4.5 GHz, a peak gain of 6.8 dBi, and an in-band gain fluctuation of less than 1.9 dB. In addition, a dual-port self-decoupled MIMO antenna is constructed by orthogonally arranging two antenna elements. Measurements demonstrate an operating band of 3.44–4.39 GHz, featuring over 23.6 dB isolation, a peak gain of 4.7 dBi, and gain fluctuation below 0.8 dB. These results confirm the antenna's compact structure, excellent diversity, and stable radiation, validating its suitability for compact 5G NR (New Radio) applications.

Single-port MS antenna

Antenna structure

The structure of the proposed single-port MS antenna is shown in Fig. 1. The antenna comprises a top MS layer, a rectangular patch layer, and a bottom ground plane. The MS consists of 3 × 3 square patch cells, with a slot etched at the center of each cell in the middle column. Both dielectric substrates are FR4 material (relative dielectric constant ε_r of 4.4 and loss angle tangent of 0.02). The rectangular patch is fed by a 50 Ω coaxial probe. The optimized geometrical parameters of the antenna are listed in Table 1.

Figure 2 shows the simulated *S*-parameters of the patch antenna with and without MS. The feed position for each configuration was optimized to ensure good radiation performance. The results demonstrate that the unloaded patch antenna operates from 4.09 to 4.22 GHz, whereas the MS-loaded counterpart operates from 3.45 to 4.5 GHz. This indicates that the MS effectively enhances the bandwidth while maintaining structural compactness.

Antenna design process using CMA

The Multilayer Solver in CST Studio Suite was utilized for the design and analysis of the antenna. First, the antenna structure was created and materials were assigned. Then, the Multilayer Solver was configured with a vacuum background and open boundary conditions. The characteristic mode count was set to four for the patch antenna and eight for both the MS and the final antenna, after which the simulation was executed. Figure 3 plots the modal significance and modal current distributions of the rectangular patch. The modal significance reflects the radiation potential, with modes having an MSv > 0.707 considered effectively excitable. As shown, the patch exhibits vertical (Mode 1, TM_{10}) and horizontal (Mode 2, TM_{01}) radiation modes at 4.3 and 5.9 GHz, respectively. Both modes display strong main lobe radiation, and exciting either mode can achieve satisfactory radiation performance. In contrast, Mode 3 (TM_{11}) and Mode 4 (TM_{20}) are spurious resonant modes with weaker radiation capabilities.

Additionally, Fig. 4 illustrates the modal significance and modal currents distributions of the initial 3 × 3 MS. As shown in Fig. 4(a), Modes 1 and 2 constitute a pair of degenerate modes. Figure 4(b) reveals that Modes 1 and 2 exhibit uniformly aligned current distributions across the MS, enabling their broadside radiation with well-defined main lobes. In contrast, Modes 3–8 display diverse current orientations and radiation patterns dominated by side-lobes, rendering them unsuitable as primary radiating modes.

To optimize radiation performance, the design aims to jointly excite a mode in the rectangular patch with its corresponding MS mode, requiring their modal currents to be aligned. To achieve this alignment, three horizontal slots were introduced into the three central patches of the initial MS. The slot widths are identical to those of the inter-unit gaps. Figure 5 illustrates the modal significance and modal current distributions of this modified MS. The results show that the slots not only separate the two degenerate modes but also reconfigure their current directions to horizontal (Mode 1) and vertical (Mode 2), respectively, thereby achieving the required current alignment for joint excitation with the patch.

https://doi.org/10.1017/S1759078726102943 Published online by Cambridge University Press

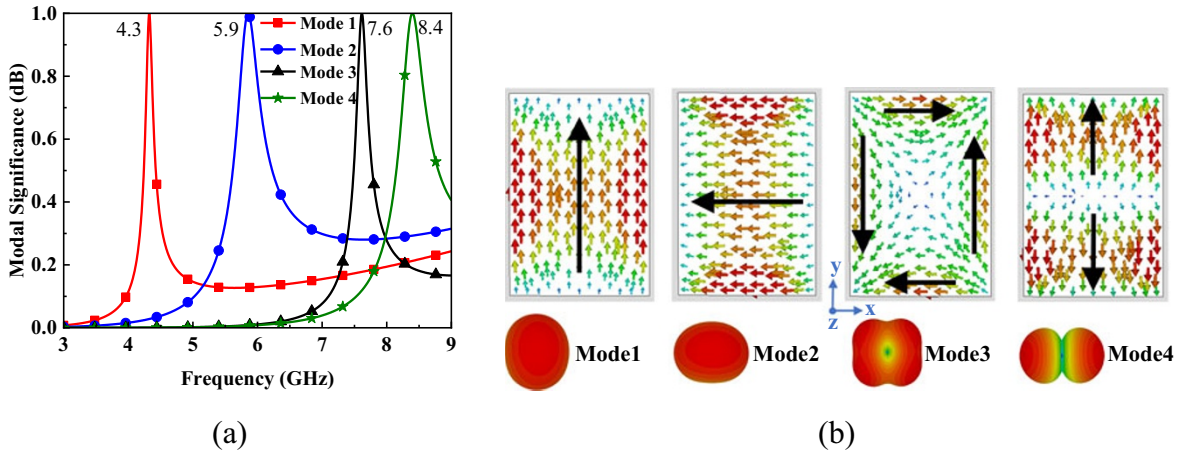


Figure 3. The CMA results of the rectangular patch. (a) Modal significance. (b) Modal currents and radiation pattern.

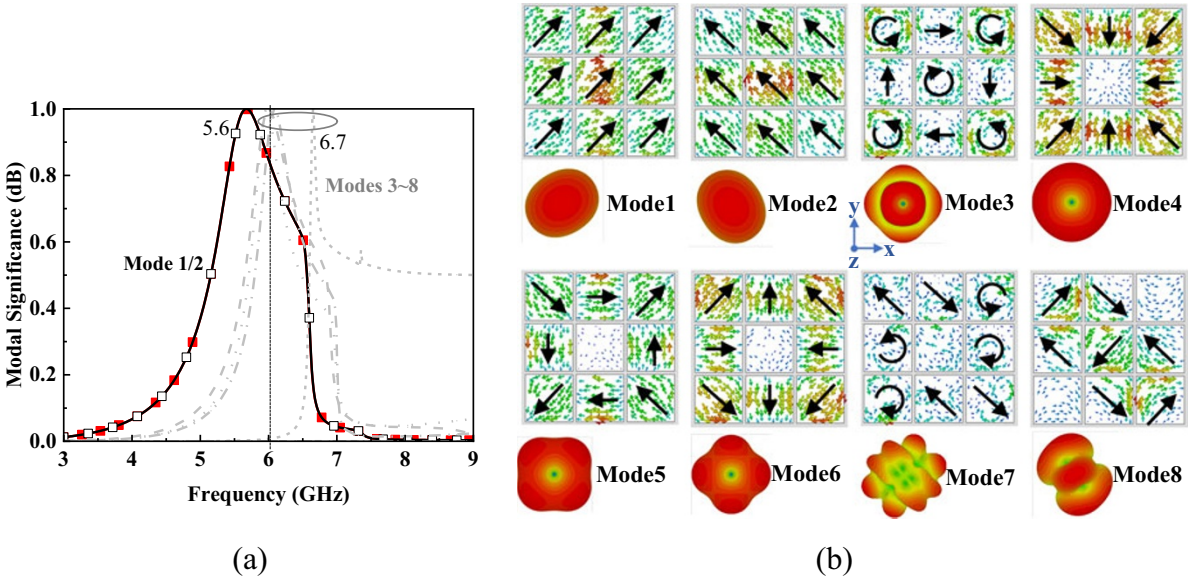


Figure 4. The CMA results of the original MS. (a) Modal significance. (b) Modal currents and radiation pattern.

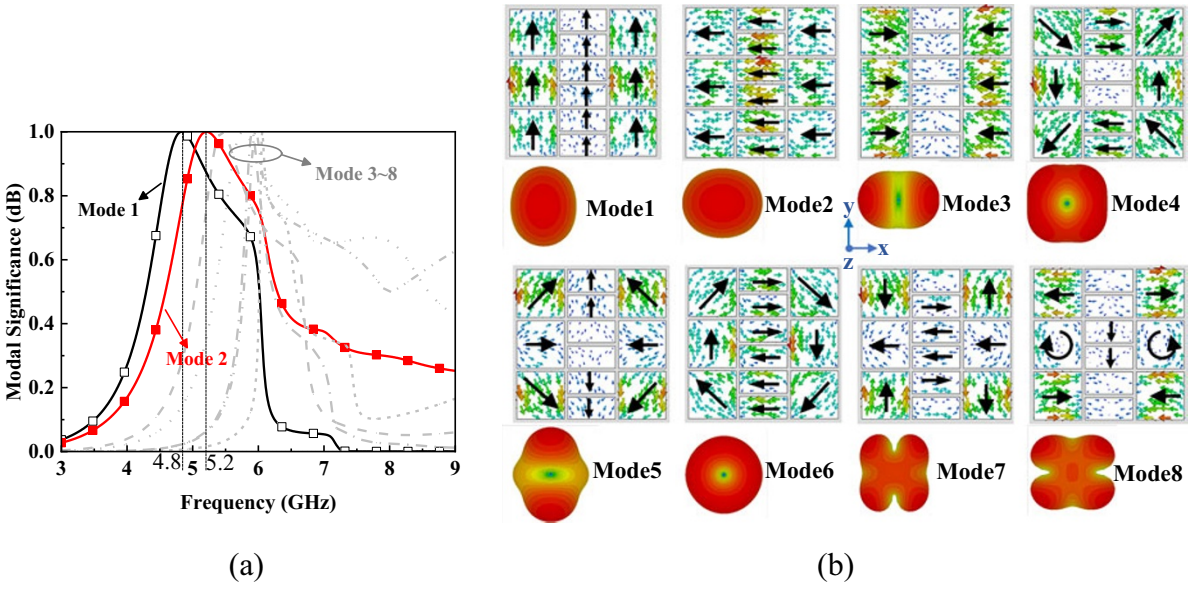


Figure 5. The CMA results of the proposed MS. (a) Modal significance. (b) Modal currents and radiation pattern.

https://doi.org/10.1017/S1759078726102943 Published online by Cambridge University Press

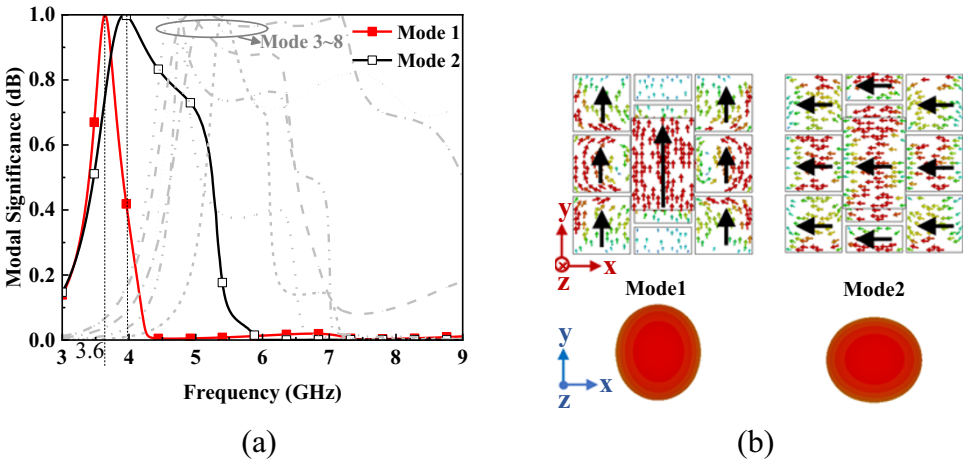


Figure 6. The CMA results of the proposed MS antenna. (a) Modal significance. (b) Modal currents and radiation pattern.

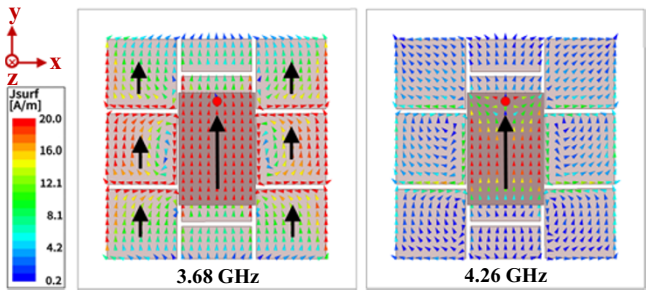


Figure 7. The current distributions at 3.68 and 4.36 GHz of the single-port MS antenna.

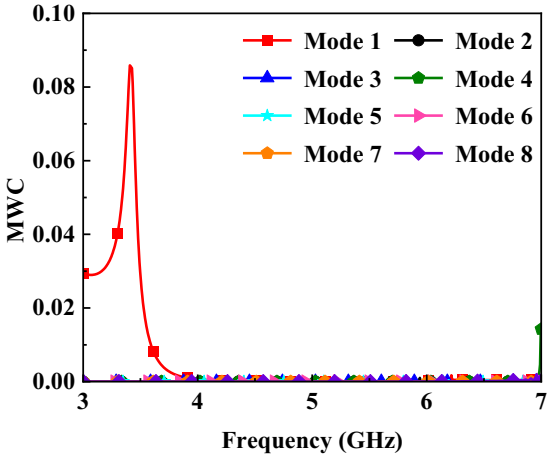


Figure 8. MWC of the proposed MS antenna.

Figure 6 shows the CMA results of the integrated MS and rectangular patch structure. To simultaneously visualize their modal current distributions, bottom views are shown inverted in Fig. 6(b). The results indicate that the integrated structure exhibits vertical (Mode 1) or horizontal (Mode 2) current distributions on both the patch and MS. Both modes maintain radiation patterns with well-defined main lobes. The modal significance curves in Fig. 6(b) show that these modes resonant at 3.64 GHz (Mode 1) and 4.0 GHz (Mode 2), respectively. Compared with the resonant frequencies of the standalone rectangular patch in Fig. 3, Mode 1 of the integrated structure resonates closer to the patch's frequency than Mode 2 does. This closer frequency alignment facilitates stronger joint excitation between the MS and the patch, which is why Mode 1 was selected for the final design.

Single-port MS antenna with coaxial feed

Based on the CMA in the previous section, a 50 Ω coaxial probe is proposed for exciting modes 1. Figure 7 illustrates the current distributions of the excited antenna at resonant frequencies of 3.68 and 4.26 GHz. As shown, the distribution at 3.68 GHz matches that of Mode 1 in the integrated patch-MS structure from Fig. 6. At 4.26 GHz, the current is primarily concentrated on the rectangular patch, which is identical to Mode 1 of the standalone patch in Fig. 3. These results are in line with the expected design.

To determine the effective excitation of the port, Fig. 8 presents the modal weighting coefficient (MWC) result which is calculated by introducing the coaxial line shown in Fig. 1 and setting it as a discrete port. It can be seen that in the frequency band around 3.6 GHz, except for Mode 1, the MWC of all other modes is close to zero. Hence, only Mode 1 is effectively excited within this frequency band, which is highly consistent with the current distribution result presented in Fig. 7.

Figure 9 compares the simulated gain of the antenna with and without the MS. The original patch antenna exhibits a peak gain of 4.8 dBi within its operational band (4.09–4.22 GHz). After integrating the MS, the gain is improved to a 4.9–6.8 dBi across an expanded bandwidth of 3.45–4.5 GHz, with a gain fluctuation of less than 1.9 dB and a flat gain curve across most of the band.

Figure 10 presents the normalized radiation patterns simulated at 3.68 and 4.26 GHz. The antenna exhibits consistent *E*- and *H*-plane radiation patterns at both frequencies, achieving quasi-omnidirectional radiation with low cross-polarization levels. The peak gains are 6.8 dBi (3.68 GHz) and 6.48 dBi (4.26 GHz), which meet the gain requirements for 5G NR applications.

Dual-port MS MIMO antenna

As illustrated in Fig. 11, two of the proposed single-port MS antennas are orthogonally arranged to form a dual-port MIMO antenna.

https://doi.org/10.1017/S1759078726102943 Published online by Cambridge University Press

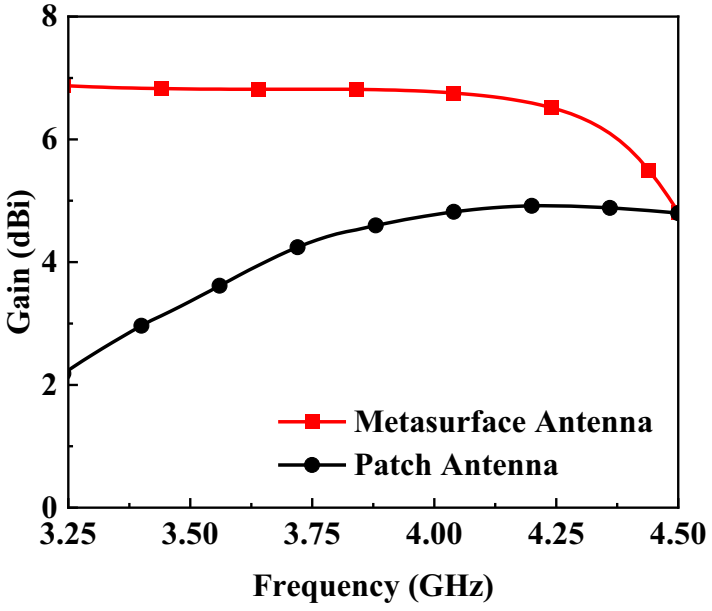


Figure 9. The simulated gain of antenna with and without MS.

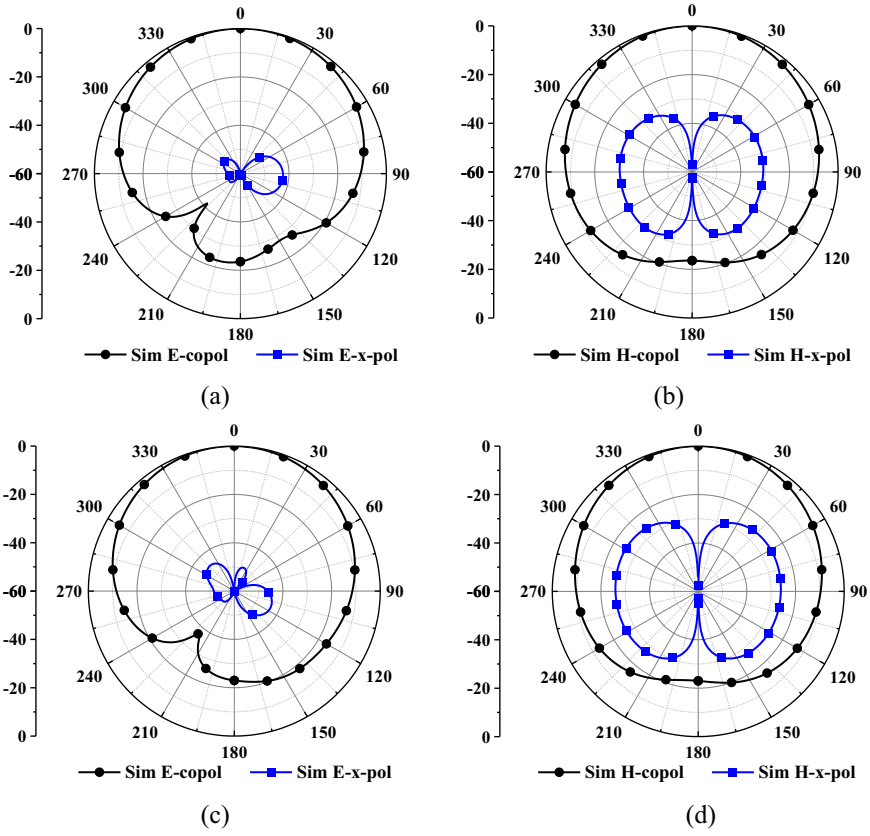


Figure 10. The simulated normalized radiation pattern of single-port MS antenna. (a) 3.68 GHz, *E*-plane. (b) 3.68 GHz, *H*-plane. (c) 4.26 GHz, *E*-plane. (d) 4.26 GHz, *H*-plane.

The edge-to-edge distance between the two MSs is 0.049 λ_0, where λ_0 is the free-space wavelength corresponding to the lower cutoff frequency of the antenna. The detailed parameters of the MIMO antenna are listed in Table 1.

Figure 12 shows the simulated *S*-parameters of the MIMO antenna. As shown, the proposed MS MIMO antenna operates from 3.44 to 4.39 GHz with an isolation greater than 23.6 dB across the entire band, demonstrating inherent decoupling. By exciting the fundamental TM_{10}, polarization diversity is achieved, enabling high isolation without additional decoupling structures.

Additionally, the current distributions of the MIMO antenna at 3.68 and 4.18 GHz are depicted in Fig. 13(a) and (b), respectively. When port 1 is excited, the current is primarily concentrated on the rectangular patch and the edge regions of the MS layer at both

https://doi.org/10.1017/S1759078726102943 Published online by Cambridge University Press

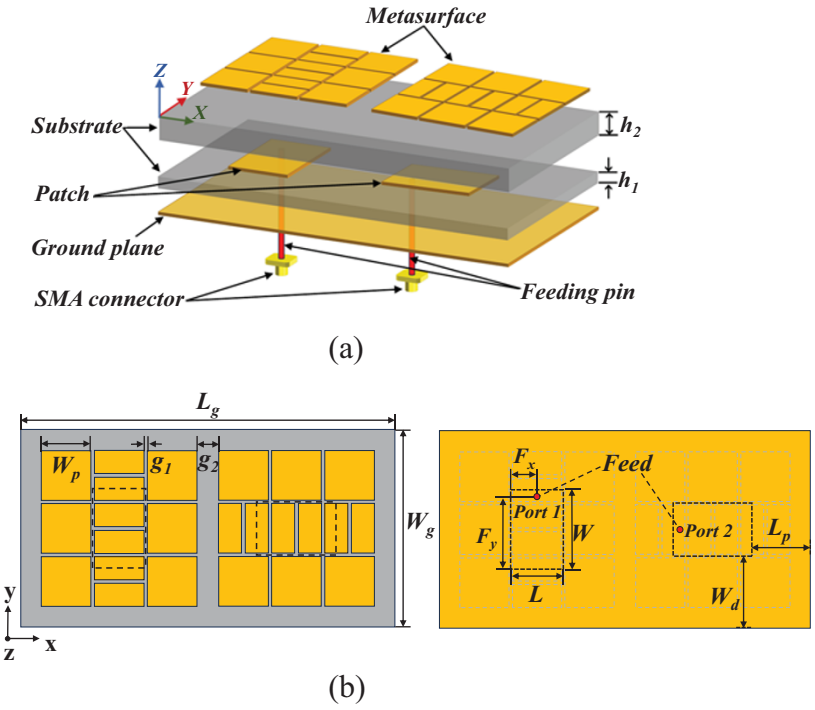


Figure 11. Geometry of the dual-port MS MIMO antenna. (a) 3D. (b) Top and bottom views.

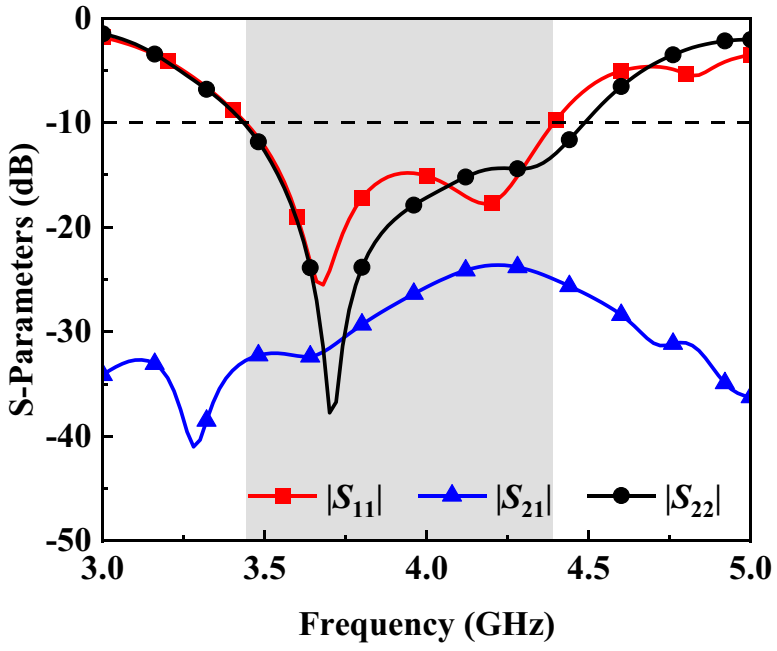


Figure 12. Simulated *S*-parameters of the MS MIMO antenna.

frequencies. In contrast, the coupled current on the neighboring antenna 2 is relatively weak.

Fabrication and experimental results

To validate the design, a prototype of the dual-port MIMO antenna was fabricated and measured. SMA-KFD5 coaxial connectors specified for DC to 6 GHz operation was adopted. The fabricated prototype and test environment are depicted in Fig. 14. The *S*-parameters were measured using an Agilent N5222A vector network analyzer, and the radiation patterns were measured in an anechoic chamber.

Figure 15 compares the measured and simulated *S*-parameters of the dual-port MIMO antenna. Good agreement is observed between the simulated and measured results, both covering an operating band of 3.44–4.39 GHz, with the measured isolation exceeding 26.25 dB across the band. The error primarily originates from manufacturing tolerances. Since the antenna consists of an MS layer and a patch layer, fabrication limitations result in a small interlayer gap at the solder joints for the SMA

https://doi.org/10.1017/S1759078726102943 Published online by Cambridge University Press

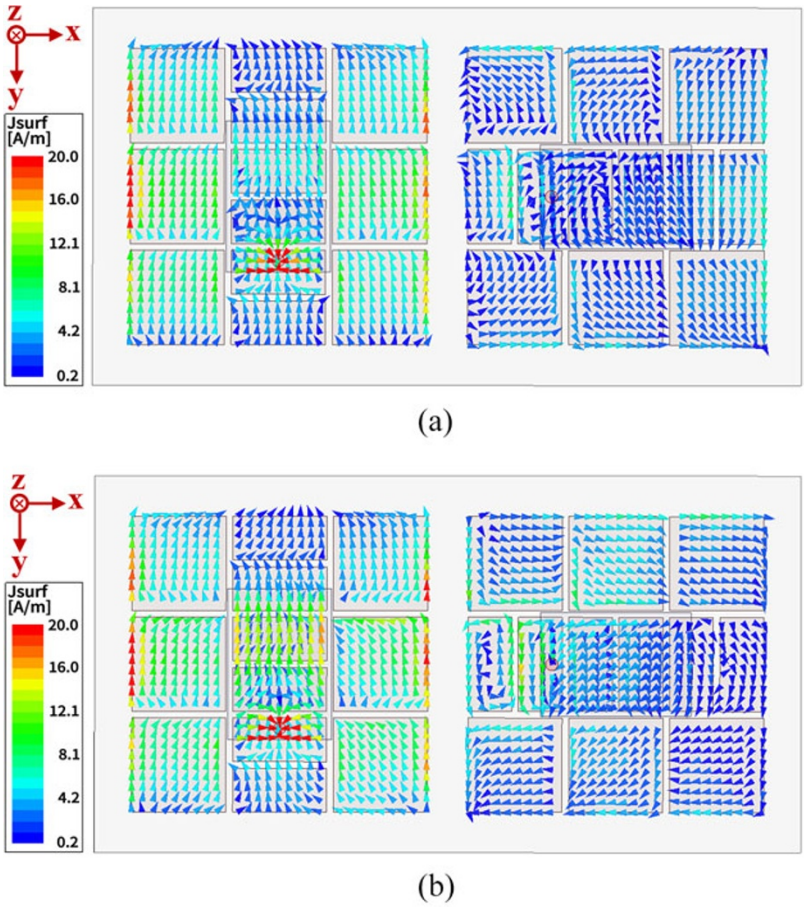


Figure 13. Current distributions of the proposed antenna at (a) 3.68 GHz and (b) 4.18 GHz.

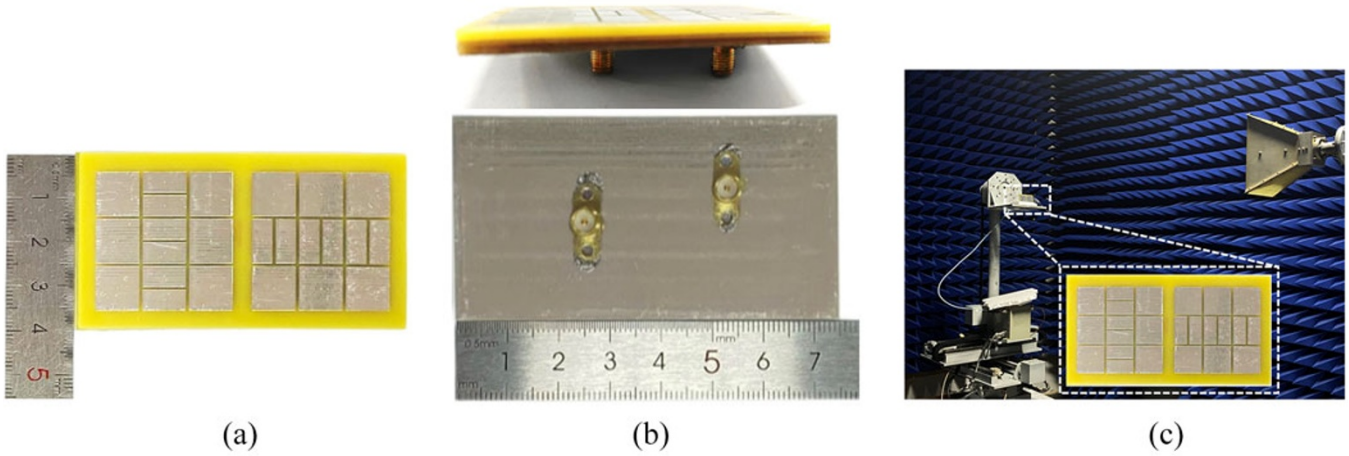


Figure 14. Fabricated antenna and test environment. (a) Top view. (b) Bottom and side view. (c) Test environment.

connector probe. This gap significantly degrades the accuracy of the measurement results. To verify this, the simulation results for a 1 mm gap between the upper and lower layers are also included in Fig. 15. It can be observed that the gap causes a frequency shift and alters the magnitude of the *S*-parameters. This confirms that the discrepancy between the measured and simulated results is mainly attributable to manufacturing tolerances.

Figure 16 compares the measured and simulated radiation patterns of the prototype at 3.68 and 4.18 GHz. When port 1 is excited, port 2 is terminated by a matched load. At the two frequencies of 3.68 GHz and 4.18 GHz, the main beam directions of the antenna in the *E*-plane are 0° and −45°, respectively, while in the *H*-plane they are both close to 0°. On the main radiation direction, the cross-polarization level is more than 20 dB lower than the co-polarization. It should be noted that within the angular range of

https://doi.org/10.1017/S1759078726102943 Published online by Cambridge University Press

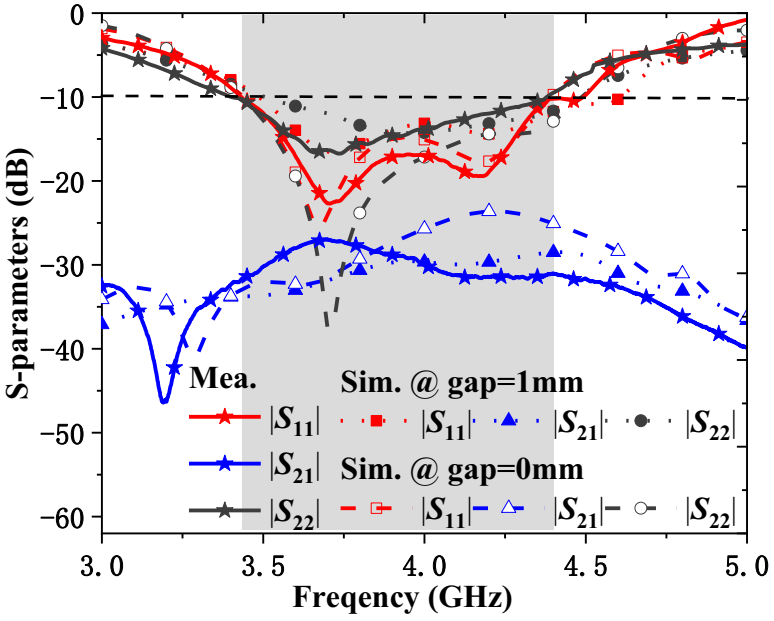


Figure 15. Simulated and measured *S*-parameters of the proposed MS MIMO antenna.

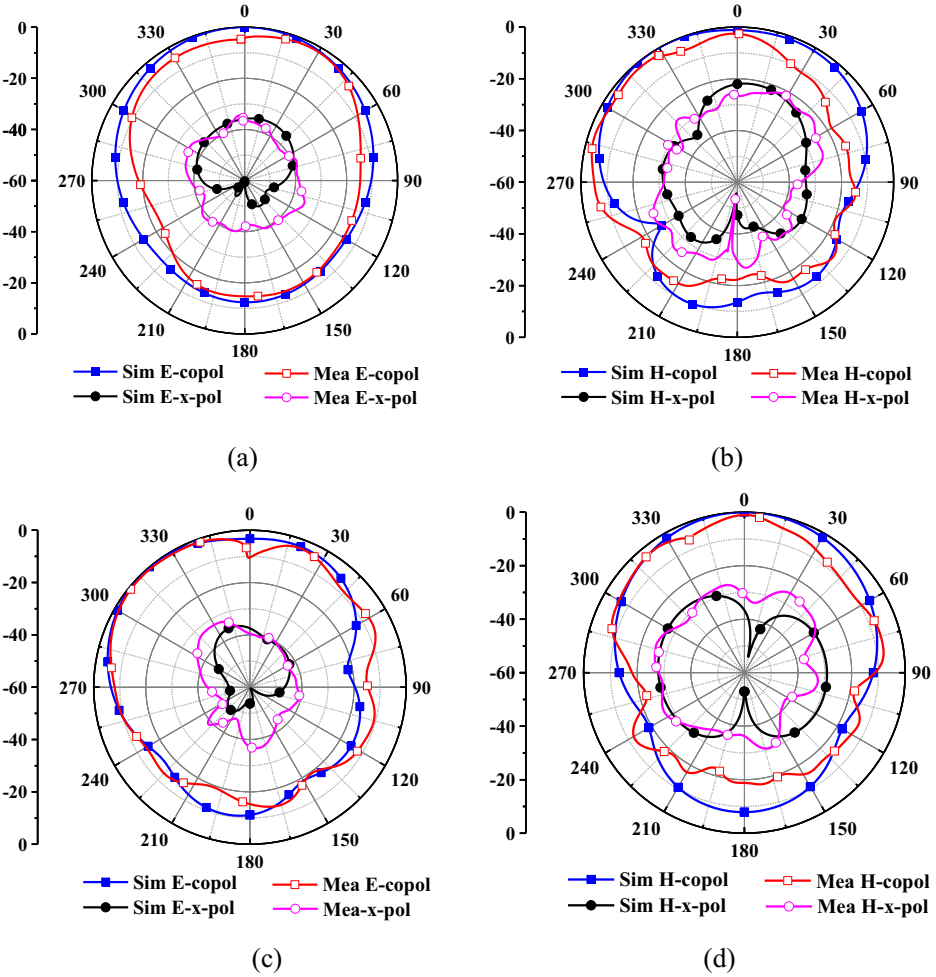


Figure 16. The simulated and measured normalized radiation pattern of MS MIMO antenna. (a) 3.68 GHz, *E*-plane. (b) 3.68 GHz, *H*-plane. (c) 4.18 GHz, *E*-plane. (d) 4.18 GHz, *H*-plane.

https://doi.org/10.1017/S1759078726102943 Published online by Cambridge University Press

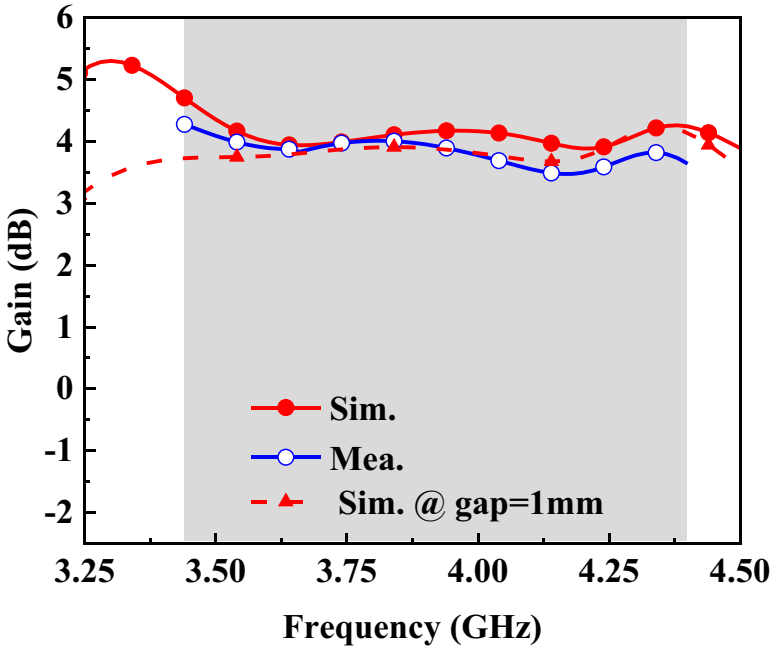


Figure 17. The simulated and measured gain of MS MIMO antenna.

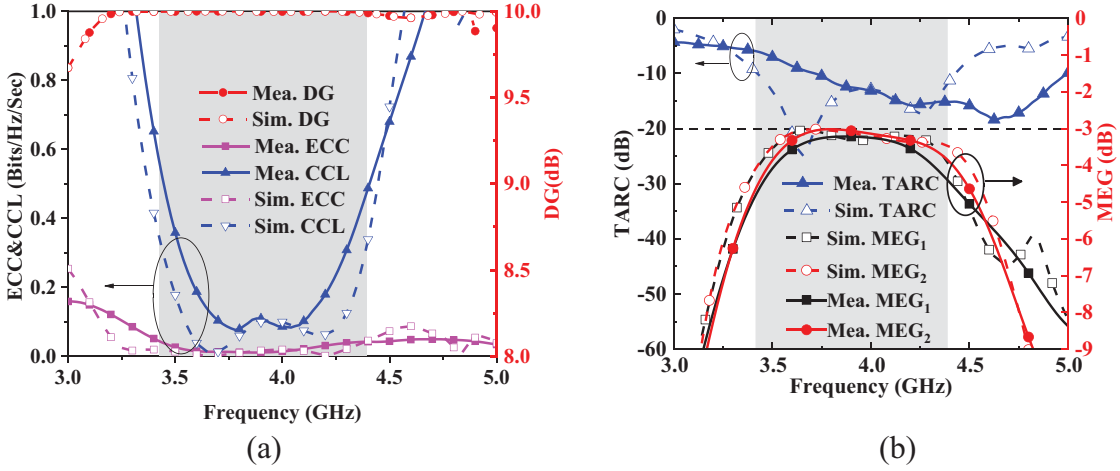


Figure 18. The indicators of MS MIMO antenna calculated from simulated and measured results. (a) ECC, CCL, and DG. (b) TARC and MEG.

120°–240° in the *E*-plane, the measured cross-polarization radiation is significantly higher than the simulation results. This discrepancy is primarily attributed to multi-path reflections and scattering from the antenna mount in the measurement environment.

Figure 17 plots the measured and simulated gain of the MIMO antenna. Over the operating band, the simulated and measured gains range from 3.9 to 4.7 dBi and 3.43 to 4.27 dBi, with fluctuations of 0.8 dB and 0.84 dB, respectively. The results demonstrate flat gain characteristics with good agreement between simulation and measurement. The discrepancy is primarily attributed to antenna fabrication tolerances as well as non-ideal measurement conditions such as cable loss, multipath interference, and gain standard uncertainty. As mentioned above, an inevitable small gap between the MS and the feed layer degrades impedance matching and introduces additional loss. To verify the impact of this fabrication imperfection, Fig. 17 also presents the simulated gain for a 1 mm interlayer gap. The results show an overall decrease in gain compared to the case without a gap, confirming that manufacturing imperfections cause errors in gain measurement.

To further evaluate the diversity characteristics and data transmission quality of this MIMO antenna, Fig. 18 presents the calculated results for envelope correlation coefficient (ECC), diversity gain (DG), total active reflection coefficient (TARC), channel capacity loss (CCL), and mean effective gain (MEG). The measured and simulated values of these indicators show good agreement. In engineering practice, the generally acceptable ranges are as follows: ECC $<$ 0.5, CCL $<$ 0.5 bits/Hz/sec, DG $>$ 6 dB (with10 dB being ideal), TARC $<$ 0 dB, and MEG $<$ −3 dB. In Fig. 18(a), within the entire operating frequency band, both measured and simulated ECC values remain below 0.05, the CCL values are under 0.48 bits/Hz/sec, and DG values exceed 9.9 dB. Meanwhile, Fig. 18(b) indicates that the TARC and MEG obtained from measurement and simulation are respectively lower

https://doi.org/10.1017/S1759078726102943 Published online by Cambridge University Press

Table 2. Comparison between the proposed and previously reported MS MIMO antennas

Ref.	Method	Dimension/λ_0^3	BW/GHz	Ports No.	Isolation/dB	GV/dBi
[25]	S-D	0.3 × 0.23 × 0.285	3.03–3.44 & 4.01–5.87 (12.6% & 37.6%)	2	>15	1.5 & 0.6
[15]	MS	1.25 × 0.83 × 0.153	2.5–2.7 & 3.4–3.6 (7.7% & 5.7%)	2	>25	-
[16]	MS	3.36 × 2.30 × 0.629	24.55–26.5 (7.6%)	4	>38	1
[24]	MS	1.05 × 0.82 × 0.05	5–6 (18.2%)	2	>25	2
[18]	S-D	1.31 × 1.31 × 0.081	24.5–29.5 (18.5%)	4	>30	-
[20]	MS	1.25 × 1.25 × 0.058	2.5–2.9 (14.8%)	4	>24	1
[23]	S-D	1.56 × 0.95 × 0.059	5.07–5.55 (9%)	2	>30	-
[21]	S-D	2.7 × 1.57 × 0.14	26–34.5 (24.8%]	2	>23	2.25
[22]	DGS MS	2.43 × 2.26 × 0.14	26–40 (42.4%)	4	>15	-
This work	S-D	0.86 × 0.46 × 0.055	3.44–4.39 (24.3%)	2	>23.6	0.8

S-D, self-decoupled; MS, MS; BW, bandwidth; GV, gain variation.

than −7 dB and −3 dB. These results confirm that the proposed MIMO antenna achieves excellent spatial multiplexing performance across the entire frequency band, ensuring reliable signal transmission.

To emphasize the superior performance of the proposed antenna, Table 2 compares its performance with those reported in previous literature. Here, λ_0 denotes the free-space wavelength corresponding to the antenna's lower cutoff frequency. The designs in [14, 20, 23] have similar profile heights but occupy a much larger area. The design in [25] has a profile height approximately five times greater than that of the proposed antenna, although it achieves the smallest footprint. The antennas in [21] and [22] have demonstrated superior performance in terms of bandwidth; however, their dimensions and profile are also significantly larger than those of this work. Consequently, the proposed design achieves significant miniaturization while also exhibiting superior gain flatness. In summary, by jointly exciting the TM_{10} mode of the rectangular patch and the MS, this work realizes a compact, high-isolation, self-decoupling MS MIMO antenna.

Conclusion

This paper proposes a gain-flattened MS MIMO antenna based on CMA. By analyzing the modal characteristics of the rectangular patch and MS, a pair of degenerate modes in the MS is separated, while the dominant mode is reconfigured into the desired TM_{10} mode. The joint excitation of the TM_{10} mode in both the rectangular patch and the MS enables broadband single-mode radiation. Furthermore, a compact MS MIMO antenna with self-decoupling capability via polarization diversity is constructed by orthogonally arranging the aforementioned single-port antennas. The proposed design exhibits isolation greater than 23.6 dB and a flat in-band gain variation of merely 0.8 dB. It operates from 3.44 to 4.39 GHz, fully encompassing the target 5G NR n48 band (3.55–3.7 GHz). A prototype of the MIMO antenna was fabricated and measured, confirming stable radiation patterns and reliable signal transmission performance. This work provides an effective solution for 5G wireless communication systems. Future work will explore bandwidth extension or dual-band configurations to address a broader range of sub-6 GHz and mmWave frequencies, thereby supporting more diverse 5G applications.

Acknowledgements. This work was supported by the National Natural Science Foundation of China (62071282) and the Fundamental Research Program of Shanxi Province (202203021211295).

Competing interests. The authors declare none.

References

1. **Yousfi AE, Abdalmalak KA, Lamkaddem A, Barrera AM, Biscontini B and Vargas DS** (2024) Miniaturized dual-polarized, high-gain, and wideband dielectric resonator antenna for low band massive MIMO applications. *Progress in Electromagnetics Research* **179**, 101–111. https://doi.org/10.2528/PIER24021303
2. **Yousfi AE, Lamkaddem A, Abdalmalak KA and Vargas DS** (2023) A broadband circularly polarized single-layer metasurface antenna using characteristic-mode analysis. *IEEE Transactions on Antennas and Propagation* **71**(4), 3114–3122. https://doi.org/10.1109/TAP.2023.3239104
3. **Elalaouy O, Ghzaoui ME and Foshi J** (2024) Mutual coupling reduction of a two-port MIMO antenna using defected ground structure. *e-Prime-Advances in Electrical Engineering, Electronics and Energy* **8**, 100557. https://doi.org/10.1016/j.prime.2024.100557
4. **Hasan MM, Islam MT, Alam T, Alzamil A and Soliman MS** (2024) Electromagnetic coupling shielding in compact MIMO antenna using symmetric T-shaped metamaterial structure for 5G communications. *Optics and Laser Technology* **169**, 110046. https://doi.org/10.1016/j.optlastec.2023.110046
5. **Wu T, Wang M-J and Chen J** (2022) Decoupling of MIMO antenna array based on half-mode substrate integrated waveguide with neutralization lines. *AEU-International Journal of Electronics and Communications* **157**, 154416. https://doi.org/10.1016/j.aeue.2022.154416
6. **Dkiouak A, Rahmani F, Ouahabi ME, Zakriti A, Baghouri M and El Mamouni A** (2024) A dual-port MIMO antenna system for 5G and Wi-Fi 6E communications using a parasitic element. *e-Prime-Advances in Electrical Engineering, Electronics and Energy* **10**, 100850. https://doi.org/10.1016/j.prime.2024.100850
7. **Ayinala KD and Sahu PK** (2021) Isolation enhanced compact dual-band quad-element MIMO antenna with simple parasitic decoupling elements. *AEU-International Journal of Electronics and Communications* **142**, 154013. https://doi.org/10.1016/j.aeue.2021.154013
8. **Geoffrey SS and Krishnan S** (2024) Broadband self-isolating MIMO antenna array for 6G IoT systems. *Optik* **315**, 172042. https://doi.org/10.1016/j.ijleo.2024.172042
9. **Hussain M, Awan WA, Alzaidi MS and Elkamchouchi DH** (2023) Self-decoupled tri band MIMO antenna operating over ISM, WLAN and C-band for 5G applications. *Heliyon* **9**(7), e17404. https://doi.org/10.1016/j.heliyon.2023.e17404

https://doi.org/10.1017/S1759078726102943 Published online by Cambridge University Press

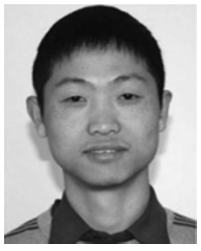
10. **Modak S, Lokam A and Farooq U** (2024) Characteristic mode based self-isolated MIMO antenna design for millimeter wave 5G communications. *AEU-International Journal of Electronics and Communications* **178**, 155257. https://doi.org/10.1016/j.aeue.2024.155257
11. **Phuong K-T, Thang NV and Thanh TB** (2024) A self-decoupling technique for isolation enhancement in closely-spaced MIMO patch antennas. *IEEE Antennas and Wireless Propagation Letters* **23**(6), 1695–1699. https://doi.org/10.1109/LAWP.2024.3367036
12. **Hung T-H, Hong NT, Nguyen QD, Tran-Viet DN and Park HC** (2024) Multi-element self-decoupled MIMO patch antenna with flexible characteristics. *IEEE Access* **12**, 21569–21575. https://doi.org/10.1109/ACCESS.2024.3362876
13. **Raza MU, Zhang K and Yan S** (2024) Metasurface-assisted mutual coupling suppression in circularly polarized MIMO antenna array for sub-6 GHz applications. *Materials & Design* **248**, 113445. https://doi.org/10.1016/j.matdes.2024.113445
14. **Wang Z, Li C and Yin Y** (2020) A meta-surface antenna array decoupling (MAAD) design to improve the isolation performance in a MIMO system. *IEEE Access* **8**, 61797–61805. https://doi.org/10.1109/ACCESS.2020.2983482
15. **Liu F, Guo J, Zhao L, Huang GL, Li Y and Yin Y** (2020) Dual-band metasurface-based decoupling method for two closely packed dual-band antennas. *IEEE Transactions on Antennas and Propagation* **68**(1), 552–557. https://doi.org/10.1109/TAP.2019.2940316
16. **Tariq S, Naqvi SI, Hussain N and Amin Y** (2021) A metasurface-based MIMO antenna for 5G millimeter-wave applications. *IEEE Access* **9**, 51805–51817. https://doi.org/10.1109/ACCESS.2021.3069185
17. **Hussain N, Jeong M-J, Abbas A and Kim N** (2020) Metasurface-based single-layer wideband circularly polarized MIMO antenna for 5G millimeter-wave systems. *IEEE Access* **8**, 130293–130304. https://doi.org/10.1109/ACCESS.2020.3009380
18. **Gerami HH and Kazemi R** 2022 A low profile and low cross-polarization metasurface antenna for 5G mm-wave applications. *2022 6th International Conference on Millimeter-Wave and Terahertz Technologies* (MMWaTT), Tehran, Iran. https://doi.org/10.1109/MMWaTT58022.2022.10172126.
19. **Ding Z, Liu Y, Ran R, Wu B, Liu C and Fu Y** (2024) Design of low-profile four-modes patterns metasurface antenna using characteristic mode analysis. *AEU-International Journal of Electronics and Communications* **175**, 155096. https://doi.org/10.1016/j.aeue.2023.155096
20. **Zeng W-F, Chen F-C and Liang Y-Z** (2025) High isolation H-plane placed metasurface MIMO antenna using characteristic field cancellation. *IEEE Transactions on Antennas and Propagation* **73**(2), 1227–1232. https://doi.org/10.1109/TAP.2024.3470909
21. **Tiwari P, Gaur MK, Kaushik M, Shastri A, Singh B and Gahlaut V** (2025) Performance evaluation of wideband dual port octagonal-shaped millimeter-wave MIMO antenna for satellite communication. *International Journal of RF and Microwave Computer-Aided Engineering* Online publication. https://doi.org/10.1155/mmce/1456913
22. **Gaur MK, Tiwari P, Kaushik M, Mishra UN, Shastri A and Gahlaut V** (2025) High-performance quad-port MIMO antenna for millimeter wave communications using metamaterial-based unit cells. *International Journal of Communication Systems* **38**, e70140. https://doi.org/10.1002/dac.70140
23. **Li H, Nan Y, Xu J-W, Chen Q and Feng TX** (2024) Self-decoupled multi-antennas with coupling modes identification and suppression. *IEEE Antennas and Wireless Propagation Letters* **23**(10), 3188–3192. https://doi.org/10.1109/LAWP.2024.3430372
24. **Wang Z, Li C, Wu Q and Yin Y** (2020) A metasurface-based low-profile array decoupling technology to enhance isolation in MIMO antenna systems. *IEEE Access* **8**, 125565–125575. https://doi.org/10.1109/ACCESS.2020.3007188
25. **Angadi S, Sharma Y, Raghava NS and Sabapathy T** (2024) A metasurface based close-proximity two-port circularly polarized MIMO antenna for mid-band sub-6 GHz 5G applications. *AEU-International Journal of Electronics and Communications* **183**, 155379. https://doi.org/10.1016/j.aeue.2024.155379
26. **Angadi S, Sharma Y, Raghava NS and Sabapathy T** (2024) A low profile circularly polarized metasurface-based ultra-wideband 4x4 MIMO antenna for 5G NR band FR2 frequencies. *AEU-International Journal of Electronics and Communications* **178**, 155282. https://doi.org/10.1016/j.aeue.2024.155282
27. **Lin FH and Chen ZN** (2017) Low-profile wideband metasurface antennas using characteristic mode analysis. *IEEE Transactions on Antennas and Propagation* **65**(4), 1706–1713. https://doi.org/10.1109/TAP.2017.2671036



Jinrong Su was born in 1981. She received the B.S. and M.S. degrees in electronic engineering and the Ph.D. degree in radio physics from Shanxi University, Taiyuan, China, in 2004, 2007, and 2017, respectively. She is currently an Associate Professor with the Department of Electronics and Information Engineering, Shanxi University. Her research interests include microwave and millimeter-wave passive device.



ShiQi Di was born in 1997. She received the B.S. degree in communication engineering and the M.S. in the Department of Information and Communication Engineering from Shanxi University, Taiyuan, China, in 2021 and 2025, respectively. Her research interests include high isolation MIMO antenna.



Xinwei Chen received the B.S. and Ph.D. degrees in electronic engineering from Shanxi University, Taiyuan, China, in 2002 and 2013, respectively. He is currently an Associate Professor with the School of Physics and Electronic Engineering, Shanxi University. His research interests include microwave and millimeter-wave passive device.



Runbo Ma was born in Changzhi, Shanxi, China, in 1974. He received the B.S., M.S., and Ph.D. degrees in electronic engineering from Shanxi University, Taiyuan, China, in 1993, 2002, and 2011, respectively. He is currently an Associate Professor with the College of Physics and Electronics, Shanxi University. His research interests include microwave and millimeter-wave integrated circuits, RFID, and microstrip antenna.

https://doi.org/10.1017/S1759078726102943 Published online by Cambridge University Press



Wenmei Zhang was born in 1969. She received the B.S. and M.S. degrees in radio technology and electromagnetic field and microwave technology from the Nanjing University of Science and Technology, Nanjing, China, in 1992 and 1995, respectively, and the Ph.D. degree in electronic engineering from Shanghai Jiao Tong University, Shanghai, China, in 2004. In 2008 and 2010, she was a Senior Visiting Scholar with the Nanyang University of Technology, Singapore. She holds 6 Chinese patent, has authored more than 150 papers in peer-reviewed journals, more than 30 papers in conference proceedings. She is currently a Professor with the School of Physics and Electronics, Shanxi University, Taiyuan, China. Her current research interests include microwave/millimeter wave integrated circuits, EMC, and microstrip antenna. Prof. Zhang served as the General Chair of "2019 Cross Strait Quad-Regional Radio Science and Wireless Technology Conference" and TPC member for multiple conferences.

https://doi.org/10.1017/S1759078726102943 Published online by Cambridge University Press